An Accurate and Preservative Quenching Data Stream Simulation Method

Eduardo Servin Torres(✉) and Qin Sheng

Department of Mathematics and Center for Astrophysics, Space Physics and Engineering Research, Baylor University, Waco, TX 76798-7328, USA
{Eduardo_Servin1,Qin_Sheng}@baylor.edu

Abstract. Quenching has been an extremely important natural phenomenon observed in many biomedical and multiphysical procedures, such as a rapid cancer cell progression or internal combustion process. The latter has been playing a crucial rule in optimizations of modern solid fuel rocket engine designs. Mathematically, quenching means the blow-up of temporal derivatives of the solution function q while the function itself remains to be bounded throughout the underlying procedure. This paper studies a semi-adaptive numerical method for simulating solutions of a singular partial differential equation that models a significant number of quenching data streams. Numerical convergence will be investigated as well as verifying that features of the solution is preserved in the approximation. Orders of the convergence will also be validated through experimental procedures. Milne's device will be used. Highly accurate data models will be presented to illustrate theoretical predictions.

1 Introduction

A key behavior observed during tumor progress, wound healing, and cancer invasion is that of rapid collective and coordinated cellular motion. Hence, understanding the different aspects of such coordinated migration is fundamental for describing and treating cancer and other pathological defects [1,2]. To reduce the number of invasive surgical procedures on patients, accurate tumor models and simulations have become crucial in the study. One of such effective models is built the nonlinear quenching partial differential equation which characterizes sudden growths of cancer cells once certain environmental criteria are reached. Similar modeling equations are frequently used in the energy industry for internal combustion machine designs [3–5].

For the sake of simplicity in formulations, we focus at an one-dimensional quenching model problem in this paper. In the circumstance, the quenching dynamics can be characterized through following modeling problem [3,6–8]:

This research is supported in part by the National Science Foundation (grant No. DMS-2318032; USA) and Simons Foundation (grant No. 1001466; USA).

H. Han and E. Baker (Eds.): SDSC 2023, CCIS 2113, pp. 228–241, 2024.
https://doi.org/10.1007/978-3-031-61816-1_16

$$\sigma(s)q_t = \frac{1}{a^2}q_{ss} + \phi(q), \quad 0 < s < 1,\ t_0 < t \le T, \tag{1.1}$$

$$q(0,t) = q(1,t) \ = \ 0, \quad t > t_0, \tag{1.2}$$

$$q(s,t_0) = q_0(s), \quad 0 \le s \le 1, \tag{1.3}$$

where $a > 0$ is the physical size of a tumor contaminated region, or a linear combustion chamber, q is the cell population index, $\phi(q) \to +\infty$ as $q \to b^-$, b is a trigging threshold of the population, and $T < +\infty$ is sufficiently large. We adopt the following degenerate and reaction functions,

$$\sigma(s) = \alpha s^{\theta}(1-s)^{1-\theta},\ \phi(q) = (b-q)^{-p}, \quad \alpha > 0,\ 0 \le \theta \le 1,\ p > 0. \tag{1.4}$$

Note that $\sigma(s) = 0$ indicates possible hidden defects within combustion chamber walls, and locations of such defects can be stochastically distributed in the spacial domain. Size of such a location set is often extremely small otherwise they can be detected in earlier stage of the manufacturing process [4,6,9]. On the other hand, the nonlinear source function $\phi(q)$ must be monotonically increasing with $\phi(0) = \phi_0 > 0$ and $\lim\limits_{q \to b^-} \phi(q) = \infty$. Our functions in (1.4) are particularly chosen to reflect aforementioned features in a relatively simple manner, and to achieve quick and successful data stream analysis in mathematics.

It has been shown that there exists a *critical value* $a^* > 0$ such that if a in (1.1) is greater than a^* then the maximal value of solution of (1.1)–(1.3) reaches its ceiling b in finite time $T_a = T(a)$. This indicates that

$$\lim_{t \to T_a^-} \max_{s \in [0,1]} q(s,t) = b \ \text{ and } \lim_{t \to T_a^-} \sup_{s \in (0,1)} q_t(s,t) = +\infty.$$

Such a phenomenon is refereed to as *quenching,* and the corresponding q is a *quenching solution.* Further, q must increase monotonically as t increases at any fixed cell location $0 < s < 1$ [10–13].

In the study of numerical combustion, the quenching stream (1.1)–(1.3) is particularly used to model combustible systems utlizing solid or liquid fuels. The ignition process starts with appearance of a outside thermal source which results in an region heating up. If the conditions are appropriate then the region will have high temperatures with drastic increase in reaction rates, eventually resulting in an explosion. The process may be found in everyday applications like automobile engine and in a more interesting setting, rocket engines. In addition to the function ω used to show certain defects in side-wall of a combustor, air bubbles contained in the fuel and, more seriously, hidden cracks in engine structures can also be formulated approximately. The partial differential equations often provide lower cost evaluations of modern engine designs before any expensive physical tests and experiments. The mathematical model and data obtained also help optimize the improvement of engines to maximize the efficiency in fuel consumptions. Needless to say, this has been one of the top concerns in the energy industry.

Our investigation is organized as follows. In the next section, we propose a second order Crank-Nicolson scheme for solving (1.1)–(1.4) on uniform spatial mesh and adaptive temporal steps. Preservations of the solution geometry such as the cell population positivity and monotonicity are studied. A proof of the convergence of the numerical solution sequence is given. A remark is stated for the more general simulation applications. Section 3 focuses on multiple numerical experiments that illustrate our analysis. Comparisons are offered with typical numerical methods in the field. Experiments are conducted on the order of accuracy of our simulation method. It is found that the method remarkably retains second order accuracy in space and first order in time, except in the quenching, or cell bursting, area as the quenching time is approached. Finally, in Sect. 4, brief concluding remarks and discussions are given for future endeavors in biomedical simulations.

2 Conservative and Convergent Algorithm

Let $b = 1$, $N \in \mathbb{N}^+$, $N \gg 1$ and $h = 1/(N+1)$. Further, let $\bar{\mathcal{D}}_N = \{s_0, s_1, \ldots, s_{N+1}\} \subset \bar{\Omega}$, where $s_k = kh$, $k = 0, 1, \ldots, N+1$. Denote $q_k^{(i)}$ as an approximation of $q(s_k, t_i)$, $k = 0, 1, \ldots, N+1$, $i = 0, 1, \ldots$ Assume that $\mathcal{D}_N \subset \bar{\mathcal{D}}_N$ be the set of interior mesh points. We approximate the spacial derivative in (1.1) through second-order central difference

$$(q_{ss})_k^{(i)} = \frac{q_{k-1}^{(i)} - 2q_k^{(i)} + q_{k+1}^{(i)}}{h^2} + \mathcal{O}(h^2), \quad s_k \in \mathcal{D}_N.$$

Drop the truncation error. Utilizing a Crank-Nicolson method we obtain the following semi-adaptive nonlinear method from (1.1)–(1.3):

$$q^{(j+1)} = \left(I - \frac{\tau_j}{2}A\right)^{-1}\left(I + \frac{\tau_j}{2}A\right)\left[q^{(j)} + \frac{\tau_j}{2}\psi\left(q^{(j)}\right)\right] + \frac{\tau_j}{2}\psi\left(q^{(j+1)}\right), \; j = 0, 1, \ldots, J, \quad (2.1)$$

$$q^{(0)} = q_0, \quad (2.2)$$

where $q^{(i)} = \left(q_1^{(i)}, q_2^{(i)}, \ldots, q_N^{(i)}\right)^\top$, $\psi = \left(\frac{\phi_1^{(i)}}{\sigma_1}, \frac{\phi_2^{(i)}}{\sigma_2}, \ldots, \frac{\phi_N^{(i)}}{\sigma_N}\right)^\top$, $A = BT \in \mathbb{R}^{N\times N}$,

$$B = \operatorname{diag}\left[\frac{1}{\sigma_1}, \frac{1}{\sigma_2}, \ldots, \frac{1}{\sigma_N}\right], \quad T = \frac{1}{a^2h^2}\begin{bmatrix} -2 & 1 & & & \\ 1 & -2 & 1 & & \\ & \cdots & \cdots & \cdots & \\ & & 1 & -2 & 1 \\ & & & 1 & -2 \end{bmatrix}, \; k = 1, 2, \ldots, N,$$

and $q_k^{(\ell)}$ is an approximation of $q(t_\ell)$, $t_\ell = \sum_{k=0}^{\ell} \tau_k$, $\ell = 0, 1, 2, \ldots, j+1$, and variable temporal steps τ_j can be determined through a proper monitoring function, such as an arc-length function [6,14]. Needless to mention, an iterative

procedure, or a linearization of the last term in (2.1), needs to be implemented for solving system (2.1), (2.2). Monotone upper-lower solution vector procedures may also be incorporated in such computations [11].

As discussed intensively in [12,15,16], solution positivity and monotonicity are among the most distinguished mathematical characteristics of singular problems such as (1.1)–(1.3), and thus (2.1), (2.2). These properties reflect proper natural behaviors of the cancer cell population growth or decay, and should be preserved throughout simulations. To the end of analysis, we let $\vee$ be one of the operations $<,\ \leq,\ >,\ \geq$. For $\alpha,\ \beta \in \mathbb{R}^N$, we assume following notations:

1. $\alpha \vee \beta$ means $\alpha_k \vee \beta_k,\ k = 1, 2, \ldots, N$;
2. $c \vee \alpha$ means $c \vee \alpha_k,\ k = 1, 2, \ldots, N$, for any $c \in \mathbb{R}$.

If $\frac{\tau_j}{h^2} \leq \frac{2a^2}{\sigma_{\max}},\ j \in \mathbb{N}$. Then matrices $I - \frac{\tau_j}{2}A,\ I + \frac{\tau_j}{2}A$ are nonsingular. Furthermore, $I + \frac{\tau_j}{2}A$ is nonnegative, $I - \frac{\tau_j}{2}A$ is monotone and inverse-positive. Under the same constraint, If there exits $\ell > 0$ such that

$$\frac{\tau_j \psi_q(\xi_k^{(j)})}{2} \leq 1,\ k = 1, 2, \ldots, N;\ Aq^{(j)} + \psi\left(q^{(j)}\right) \geq 0,\ j = 0, 1, \ldots, \ell,$$

then the solution sequence, $q^{(0)},\ q^{(1)}, \ldots, q^{(\ell)}, \ldots$, generated by (2.1), (2.2) are monotonically increasing. To see the above, from (2.1) we may observe that

$$\begin{aligned} q^{(j+1)} - q^{(j)} &= \left(I - \frac{\tau_j}{2}A\right)^{-1}\left(I + \frac{\tau_j}{2}A\right)\left[q^{(j)} + \frac{\tau_j}{2}\psi\left(q^{(j)}\right)\right] \\ &+ \frac{\tau_j}{2}\psi\left(q^{(j+1)}\right) - q^{(j)} = \left(I - \frac{\tau_j}{2}A\right)^{-1} w^{(j)}, \end{aligned} \tag{2.3}$$

where

$$w^{(j)} = \tau_j A q^{(j)} + \tau_j \psi\left(q^{(j)}\right) + \frac{\tau_j}{2}\left(I - \frac{\tau_j}{2}A\right)\psi_q\left(\xi^{(j)}\right)\left(q^{(j+1)} - q^{(j)}\right).$$

Substitute the above back into (2.3) to yield

$$q^{(j+1)} - q^{(j)} = \tau_j\left[I - \frac{\tau_j}{2}\psi_q\left(\xi^{(j)}\right)\right]^{-1}\left(I - \frac{\tau_j}{2}A\right)^{-1}\left[Aq^{(j)} + \psi\left(q^{(j)}\right)\right].$$

Therefore $\left[I - \frac{\tau_j}{2}\psi_q\left(\xi^{(j)}\right)\right]^{-1}$ is nonnegative. This ensures the anticipated monotonicity $q^{(j+1)} \geq q^{(j)}$.

Theorem A. *The semi-adaptive method* (2.1), (2.2) *is convergent.*

Proof. Assume that $Q_k^{(\ell)}$ be the exact solution of (1.1)–(1.3), then

$$Q^{(j+1)} = \left(I - \frac{\tau_j}{2}A\right)^{-1}\left(I + \frac{\tau_j}{2}A\right)\left[Q^{(j)} + \frac{\tau_j}{2}\psi\left(Q^{(j)}\right)\right] + \frac{\tau_j}{2}\psi\left(Q^{(j+1)}\right) + \mathcal{O}\left(\tau_j^2\right).$$

Subtracting (2.1) from the above and denote $\varepsilon^{(\ell)} = Q^{(j+1)} - q^{(j+1)}$, we find that

$$\varepsilon^{(j+1)} = \left(I - \frac{\tau_j}{2}A\right)^{-1}\left(I + \frac{\tau_j}{2}A\right)\left\{\varepsilon^{(j)} + \frac{\tau_j}{2}\left[\psi\left(Q^{(j)}\right) - \psi\left(q^{(j)}\right)\right]\right\} + \frac{\tau_j}{2}\left[\psi\left(Q^{(j+1)}\right) - \psi\left(q^{(j+1)}\right)\right] + \mathcal{O}\left(\tau_j^2\right). \tag{2.4}$$

Note that

$$\psi\left(Q^{(\ell)}\right) - \psi\left(q^{(\ell)}\right) = \psi_q\left(\xi^{(\ell)}\right)\varepsilon^{(\ell)},$$

where elements of $\xi^{(\ell)}$, $\xi_k^{(\ell)} \in \left(\min\left\{q_k^{(\ell)}, Q_k^{(\ell)}\right\}, \max\left\{q_k^{(\ell)}, Q_k^{(\ell)}\right\}\right)$, $k = 1, 2, \ldots, N$. Recall (2.1). From (2.4) we obtain immediately that

$$\varepsilon^{(j+1)} = \left(I - \frac{\tau_j}{2}E_1^{(j+1)}\right)^{-1}\left(I - \frac{\tau_j}{2}A\right)^{-1}\left(I + \frac{\tau_j}{2}A\right)\left(I + \frac{\tau_j}{2}E_0^{(j)}\right)\varepsilon^{(j)} + \mathcal{O}\left(\tau_j^2\right).$$

It follows readily that

$$\left\|\varepsilon^{(j+1)}\right\|_2 = \left\|\left(I - \frac{\tau_j}{2}E_1^{(j+1)}\right)^{-1}\left(I - \frac{\tau_j}{2}A\right)^{-1}\left(I + \frac{\tau_j}{2}A\right)\left(I + \frac{\tau_j}{2}E_0^{(j)}\right)\varepsilon^{(j)}\right\|_2 + C_0\tau_j^2,$$

where $C_0 > 0$ is a constant. Using norm properties,

$$\left\|\varepsilon^{(j+1)}\right\|_2 \le (1 + M\tau_j)\left\|\varepsilon^{(j)}\right\|_2 + C\tau_j^2,$$

where constants $M,\ C \in \mathbb{R}^+$. Use the above inequality recursively. We acquire that

$$\begin{aligned}\left\|\varepsilon^{(j+1)}\right\|_2 &\le (1 + M\tau_j)(1 + M\tau_{j-1})\left\|\varepsilon^{(j-1)}\right\|_2 + (1 + M\tau_j)C\tau_{j-1}^2 + C\tau_j^2 \\ &= (1 + M\tau_j)...(1 + M\tau_0)\left\|\varepsilon^{(0)}\right\|_2 + C\tau_0^2(1 + M\tau_j)...(1 + M\tau_1) + \cdots \\ &\quad + C\tau_{j-1}^2(1 + M\tau_j) + C\tau_j^2 \\ &= C\tau_0^2(1 + M\tau_j)\cdots(1 + M\tau_1) + \cdots + C\tau_{j-1}^2(1 + M\tau_j) + C\tau_j^2,\end{aligned}$$

since $\varepsilon^{(0)} = 0$ due to the initial value used. We further observe that

$$\begin{aligned}&C\tau_0^2(1 + M\tau_j)\cdots(1 + M\tau_1) + \cdots + C\tau_{j-1}^2(1 + M\tau_j) + C\tau_j^2 \\ &\quad = C\tau_0^2(1 + M\tau_0^*)^j + C\tau_1^2(1 + M\tau_1^*)^{j-1} + \cdots + C\tau_{j-1}^2(1 + M\tau_{j-1}^*) + C\tau_j^2,\end{aligned}$$

where τ_i^* for $i = 0, 1, \ldots, j-1$ are adaptive time steps used. Recursively, we obtain that

$$\begin{aligned}&C\tau_0^2(1 + M\tau_0^*)^j + C\tau_1^2(1 + M\tau_1^*)^{j-1} + \cdots + C\tau_{j-1}^2(1 + M\tau_{j-1}^*) + C\tau_j^2 \\ &\quad \le C\tau_0^2 e^{b_0 T} + C\tau_1^2 e^{b_1 T} + \cdots + C\tau_{j-1}^2 e^{b_{j-1} T} + C\tau_j^2,\end{aligned}$$

where b_i for $i = 0, 1, \ldots, j-1$ are positive constants such that $\tau_i^* = b_i \tau_{b_i}^*$ and $\tau_{b_i}^* = T/N$. Let us take the b_k that gives us the maximum of b_i in the above. Therefore,

$$C\tau_0^2 e^{b_0 T} + C\tau_1^2 e^{b_1 T} + \cdots + C\tau_{j-1}^2 e^{b_{j-1} T} + C\tau_j^2 \le C e^{b_k T}(\tau_0^2 + \tau_1^2 + \cdots + \tau_{j-1}^2 + \tau_j^2).$$

Now, denote $Ce^{b_k T} = \tilde{C}$ and set $\tau_m = \max\limits_{\ell} \tau_\ell \ll 1$. From above investigations, we have

$$\left\| \varepsilon^{(j+1)} \right\|_2 \le \tilde{C}\tau_m \left(\tau_0 + \tau_1 + \cdots + \tau_{j-1} + \tau_j\right) = \tilde{C}\tau_m T \to 0$$

as $h, \tau_m \to 0$. This ensures the expected convergence. ■

Remark 2.1. As an extension of the theorem, we may also prove that for any given $\ell \in \mathbb{N}$ and beginning solution $q^{(\ell)} < 1$, if

$$\gamma_j = \frac{\tau_j}{h^2} \le \frac{2a^2}{\sigma_{\max}};\ \frac{\tau_j}{2}\psi_q(\xi_k^{(j)}) \le 1,\ k = 1, 2, \ldots, N;\ Aq^{(j)} + \psi\left(q^{(j)}\right) \ge 0,\ \ j = \ell,\ \ell+1, \ell+2, \ldots,$$

then the vector solution sequence $q^{(\ell)}$, $q^{(\ell+1)}$, $q^{(\ell+2)}, \ldots$, generated by the semi-adaptive scheme (2.1), (2.2) increases monotonically until unity is exceeded by a component of the vector (that is, until quenching occurs) or converges to a steady solution of the problem (1.1)–(1.3). In the latter case, we do not have a quenching solution.

Remark 2.2. We note that the last set of inequalities used in Remark 2.1 has been ensured at least for the case $\ell = 0$ and $q^{(0)}$. It seems that the solution monotonicity requires more rigorous constraints than those for the numerical convergence. This additional numerical feature is definitely justified for ensuring expected quenching-blow up phenomena. However, the quenching data monotonicity requirement has also made applications of nonuniform spacial grids much more challenging.

Remark 2.3. The simulation method (2.1), (2.2) is numerical stable in the von Neumann sense [17]. Since the scheme is often solved via a suitable linearization of the nonlinear function ψ, the simulation method is also convergent due to a natural conclusion of the Lax equivalence theorem. However, in the circumstance, the order of convergence remains to be determined [11,18].

3 Order of Convergence and Simulation Results

The order of convergence $r > 0$ of a consistent numerical method is defined through the error estimate,

$$\left\| q^{(j)} - q(t_j) \right\|_p = \mathcal{O}(h^r), \quad h \to 0^+,\ j \in \{0, 1, \ldots, J\}, \tag{3.1}$$

in the p-norm ($p \geq 1$). Since (3.1) is in general difficult to use, r is often replaced practically by the order of the truncation error, or defect, of the underlying method [5,18,19].

Theorem B. *The order of convergence of the semi-adaptive method* (2.1), (2.2) *is quadratic in the maximum norm.*

Proof. Since our simulation method (2.1), (2.2) is proven to be convergent and numerical stable according to the Lax equivalence theorem, we know that $r > 0$. To estimate such an order via a defect function, we notice that

$$\sigma(s)q_t - \frac{1}{a^2}q_{ss} - \phi(q) = 0$$

due to (1.1). Further, let $\tau,\ h$ be the temporal and spacial discretization parameters, respectively. Based on the forward temporal difference and central spacial difference, we acquire from the above equation that

$$\sigma(s_k)\left(\frac{q_k^{(j+1)} - q_k^{(j)}}{\tau} + \mathcal{O}(\tau)\right) - \frac{1}{a^2}\left(\frac{q_{k+1}^{(j)} - 2q_k^{(j)} + q_{k-1}^{(j)}}{h^2} + \mathcal{O}(h^2)\right) - \phi(q_k^{(j)}) = 0,$$
$$k = 1, 2, \ldots, N;\ j = 0, 1, \ldots, J.$$

Recall the Courant constraint $\tau/h^2 = \mathcal{O}(1)$ for thermodynamic finite difference approximations [18]. Then the above equalities imply that the pointwise defect

$$d_k^{(j)} = \sigma(s_k)\frac{q_k^{(j+1)} - q_k^{(j)}}{\tau} - \frac{1}{a^2}\frac{q_{k+1}^{(j)} - 2q_k^{(j)} + q_{k-1}^{(j)}}{h^2} - \phi(q_k^{(j)}) = \mathcal{O}(h^2), \quad (3.2)$$
$$k = 1, 2, \ldots, N;\ j = 0, 1, \ldots, J.$$

Therefore $\left\|d^{(j)}\right\|_\infty = \mathcal{O}(h^2)$ as $h \to 0^+,\ j \in \{0, 1, \ldots, J\}$. Hence the order of convergence of the data stream method (2.1), (2.2) is quadratic in the maximum norm. ■

Remark 3.1. The order of convergence of the semi-adaptive simulation method (2.1), (2.2) is $r = 1.5$ in the Euclidean norm.

This can be seen readily from (3.2). We observe that $d_k^{(j)} \approx c_{k,j}h^2$, where $c_{k,j} > 0$ is a constant, $k = 1, 2, \ldots, N;\ j = 0, 1, \ldots, J$ Now,

$$\left\|d^{(j)}\right\|_2 \approx c_j\sqrt{Nh^4} = c_j\sqrt{N}h^2 \leq \frac{c_j}{\sqrt{h}}h^2 = c_j h^{3/2},\ j = 0, 1, \ldots, J,$$

where $c_j,\ j = 0, 1, \ldots, J$, are positive constants. This completes our derivation.

Although a replacement definition based on defects cannot warrant (3.1), it offers straightforward estimate and is extremely convenient to use. In fact, the actual order of convergence defined in (3.1) is often lower than that calculated via the replacement definition [20,21]. Since a quadratic or higher convergence

is often favorable to applications, such as those in cell migration model simulations [22], it is extremely meaningful to investigate and ensure the quality of convergence of (2.1), (2.2).

Fortunately, the task is possible through a generalized Milne device. This is stated through the following remark.

Remark 3.2. The order of convergence of the semi-adaptive simulation method (2.1), (2.2) is quadratic based on computational verifications via a generalized Milne device.

To demonstrate the result, we let q_h^τ denote the quenching solution with temporal steps $\tau \in \{\tau_1, \tau_2, \ldots, \tau_J\}$ h being the uniform spatial step. Further, let $q_{h/2}^\tau$ be the numerical solution with halved spatial step size $h/2$. Likewise, we define $q_{h/4}^\tau$ by a similar argument. It follows that a generalized Milne formula can be built for estimating the point-wise order of convergence via

$$r_k^{(j)} = \frac{1}{\ln(2)} \ln \left| \frac{\left(q_k^{(2j)}\right)_{h/2}^\tau - \left(q_k^{(j)}\right)_h^\tau}{\left(q_k^{(4j)}\right)_{h/4}^\tau - \left(q_k^{(2j)}\right)_{h/2}^\tau} \right|, \quad k = 1, 2, \ldots, N;\ j = 1, 2, \ldots, J, \tag{3.3}$$

given that the denominator is nontrivial [20]. Stretch the data from computational space $[0, 1]$ to original physical space $[0, 5]$ [19]. A surface of function $r_k^{(j)}$ is shown in Fig. 1. The surface can be viewed as a computational order of convergence spreading the entire space-time domain considered. Although the evaluation takes place on three "consecutive" meshes in the space, it can be conveniently extended for multidimensional cases. Detailed values of $r_k^{(j)}$ immediately before the quenching time are given in Table 1.

There is little surprise that such a surface of r obtained is not linear due to the strong quenching-blow up singularity of the quenching problem. We may notice the dramatic decay of the point-wise order of convergence from quadratic to one half in the quenching neighborhood near T_a. The phenomenon is consistent with existing discussions [15,19,20]. We note that if the variable Courant numbers $\gamma_j = \tau_j/h^2 \le a^2\phi_{\min}$, $j = 1, 2, \ldots, J$, then a quadratic convergence in space implies a linear convergence in time, that is,

$$\left\| q^{(j)} - q(t_j) \right\|_2 = \mathcal{O}(\tilde{\tau}), \quad \tilde{\tau} \to 0^+,\ j \in \{0, 1, \ldots, J\}, \tag{3.4}$$

where $\tilde{\tau} = \max_{0 \le j \le J} \tau_j$.

Formula (3.3) can be also extended via any standard p-norm, that is,

$$r_\ell^{(j)} = \frac{1}{\ln(2)} \ln \frac{\left\| (q^{(2j)})_{h/2}^\tau - (q^{(j)})_h^\tau \right\|_p}{\left\| (q^{(4j)})_{h/4}^\tau - (q^{(2j)})_{h/2}^\tau \right\|_p}, \quad 1 \le p \le \infty,\ j = 1, 2, \ldots, J. \tag{3.5}$$

On the other hand, if us consider a subset of the numerical solution sequence

$$Q_{m,n} = \left\{ q^{(m)}, q^{(m+1)}, \ldots, q^{(j)}, \ldots, q^{(n)} \right\} \subseteq \left\{ q^{(0)}, q^{(1)}, \ldots, q^{(j)}, \ldots, q^{(J)} \right\},$$

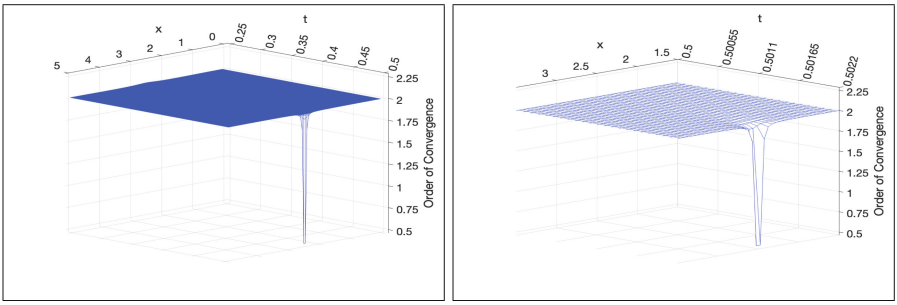

Fig. 1. [LEFT] Surface plot of the point-wise order of convergence of the numerical solution v by (2.1), (2.2). Formula (3.3) is employed.; [RIGHT] A locally enlarged surface plot of the left image near the quenching singularity. It can be observed that the the point-wise order is approximately quadratic except in a small area around the quenching data location which is at (s^*, T_a). Though the order decreases dramatically in such a small area, it still stays above 0.5 which indicates a satisfactory data reliability even in the tumor cell population blow-up area.

Table 1. The order of convergence of the solution $q(s,t)$ calculated via (3.3) at ten different s_j locations right before data quenching. Note the order is approximately 2 everywhere except around $s = 2.5$ which decreases to 0.5 due to the quenching singularity. These results are consistent with the existing theory [10–13].

s_j	order of convergence
2.02970297	1.99667070
2.12871287	1.99507152
2.22772277	1.99132454
2.32673267	1.97782804
2.42574257	1.80611369
2.52475247	0.50791656
2.62376237	1.95012804
2.72277227	1.98707873
2.82178217	1.99364935
2.92079207	1.99601168
3.01980198	1.99715469

where $0 \le m < n \le J$, then the following $(n-m+1)$-dimensional vectors

$$w_k = \left(q_k^{(m)}, q_k^{(m+1)}, \ldots, q_k^{(j)}, \ldots, q_k^{(n)}\right)^\intercal, \ k = 1, 2, \ldots, N,$$

can be defined. Therefore (3.5) can be simplified to

$$r_{\ell,k} = \frac{1}{\ln(2)} \ln \frac{\left\| w^{\tau}_{k,h/2} - w^{\tau}_{k,h} \right\|_{\ell}}{\left\| w^{\tau}_{k,h/4} - w^{\tau}_{k,h/2} \right\|_{\ell}}, \quad 1 \le \ell < \infty, \ k = 1, 2, \ldots, N. \tag{3.6}$$

The above new formula is extremely convenient to use in cell simulation experiments. It also provides an effective order of convergence estimate spanning from t_m to t_n at each spacial location s_k, $k = 1, 2, \ldots, N$. It reflects the quality of performance of the algorithm dynamically in different stage of stream simulations.

Again, for the simplicity of illustration, let us consider the case with an uniform Courant number $\gamma = \tau/h^2 = 1.0201$ with $h = 1/101$. In Fig. 2, we present order estimates based on temporal intervals $[t_0, t_{1674}]$, $[t_{1675}, t_{3348}]$ and $[t_{3349}, t_{5023}]$ in Fig. 2. The spectral norm ($\ell = 2$) is used. It is found that the order is persistently stay at two, while decays repeatedly around the quenching-blow up location $s^* = 2.5$ in the last stage. We also notice that the order is slightly higher in the first stage probably due to the excellent stability of the argorithm.

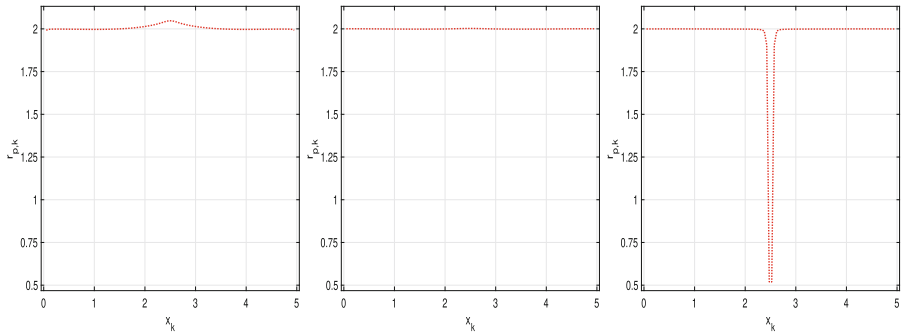

Fig. 2. Simulations of the order of convergence estimates based on formula (3.6). The three temporal stages used are $[t_0, t_{1674}]$, $[t_{1675}, t_{3348}]$ and $[t_{3349}, t_{5023}]$, respectively.

Finally, we may show a simulated quenching solution q and its rate-of-change function q_t. To do so, we may linearize (2.1), (2.2) to the following.

$$q^{(j+1)} = \left(I - \frac{\tau_j}{2} A\right)^{-1} \left(I + \frac{\tau_j}{2} A\right) \left[q^{(j)} + \frac{\tau_j}{2} \psi\left(q^{(j)}\right)\right] + \frac{\tau_j}{2} \psi\left(\omega^{(j+1)}\right), \ j = 0, 1, \ldots, J, \tag{3.7}$$

$$q^{(0)} = q_0, \tag{3.8}$$

where

$$\omega^{(j+1)} \approx q^{(j+1)} = q^{(j)} + \tau_j \left[A q^{(j)} + \psi(q^{(j)})\right].$$

Consider a typical nonstochastic reaction function of the type (1.4) with $p = 1$. Let us keep $\tau^{(\ell)}$ to be uniformly for simplicity in simulations. A fixed physical space of $a = 5$ is selected.

Figure 3 shows the simulated solution and its corresponding temporal derivative function for the final 223 temporal levels before the quenching at $T_5 \approx 0.50111987$ ($J = 723$ temporal steps are used in the full simulation). Linearized scheme (3.7), (3.8) is utilized. A single point quench is observed at $s = 2.5$ as predicted [5,10,24]. The numerical solution is clearly nonnegative, and monotonically increasing as time t increases at any $s \in (0, a)$. It can also be observed that while the solution q remains bounded throughout the computation, its rate of change, that is, the temporal derivative function q_t seems to shoot to the infinity at $s = 2.5$ as data quenching is approached [9,15,22].

In the thermal physics, the phenomenon indicates that a combustion is ignited when the rate of change of the fuel temperature in a combustion chamber tends to be unbounded. In Table 2, we list maximal values of q and q_t in ten representative time levels, including six levels immediately before the quenching-blow up. We note that τ_j becomes variable after $j = 500$ due to the kick-in of the adaptation. The patterns of the data agree very well with those given in [5,10].

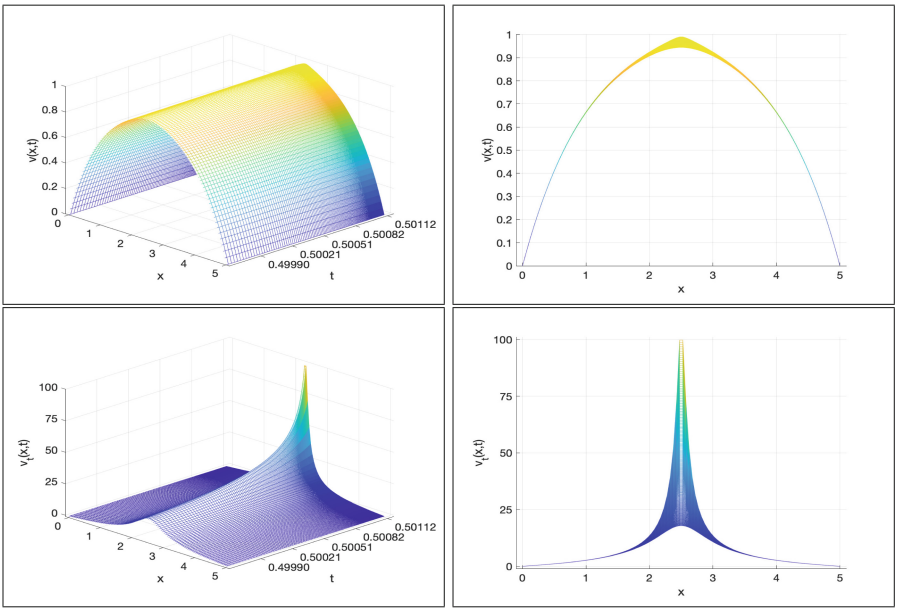

Fig. 3. Surface plots of the numerical solution q of (3.7)–(3.8) (first row), the corresponding rate derivative q_t (second row) for the last 223 temporal steps immediately before quenching. It can be observed that $T_5 \approx 0.50111987$, $\max_{0\le s\le 5, 0\le t\le T_a} q(s,t) = q(2.5, T_a) \approx 0.99008661$ and $\max_{0\le s\le 5, 0\le t\le T_a} q_t(s,t) = q_t(2.5, T_a) \approx 99.77142399$.

Our simulation strategy is the following. (i) A uniform time step τ is used until the solution almost quenches, for example, as the value $\max\limits_{0\le s\le a} q(x,t)$ reaches 0.950. (ii) Then the sequence of adaptive time steps, $\{\tau_j\}$, begins through

$$\tau_j = \max\left\{\min_j\left\{\tau_{j-1}, c_0 \min_k\left\{\left(1-q_k^j\right)^2\right\}\right\}, m_0\right\},$$

where $c_0 > 0$ is a suitable speed controller, and m_0 is a minimum step size that may keep the ratio of τ_j/τ_{j-1} being bounded and smooth [13,14]. A quadratic function is being used to reflect the nonlinearity and determine the next step size which allows the actual quenching singularity to drive the process. The above monitoring function developed is different from classical arc-length formulas and is highly satisfactory.

We plot the variable temporal steps generated as well as the performance ratio τ_j/τ_{j-1} in final 223 advancements in Fig. 4. It can be observed that while both q_j and $(q_t)_j$ increases monotonically, τ_k decreases monotonically due to our effective grid adaptation mechanism. In fact, the decay of τ_j is at a logarithmic rate.

Table 2. Maximal values of the solution $q(s,t)$ and its temporal derivative function $q_t(s,t)$ at ten different time levels before quenching-blow up. Note that the temporal adaptation starts at $j = 500$. Both values increase monotonically, with the latter increases exponentially immediately before the quenching-blow up. The results agree with known results given in [3,5,21,23].

j	t_j	$\max\limits_{0\le s\le a} q(s,t_j)$	$\max\limits_{0\le s\le a} q_t(s,t_j)$
10	0.01	0.00904086	1.00963768
100	0.1	0.10445547	1.11733601
500	0.49724053	0.91046311	11.22462715
700	0.50109449	0.98766458	81.72099321
715	0.50111365	0.98937234	94.91275358
716	0.50111474	0.98947743	95.86501759
717	0.50111580	0.98958149	96.82691747
718	0.50111685	0.98968452	97.79855187
719	0.50111787	0.98978654	98.78002048
720	0.50111887	0.98988755	99.77142399

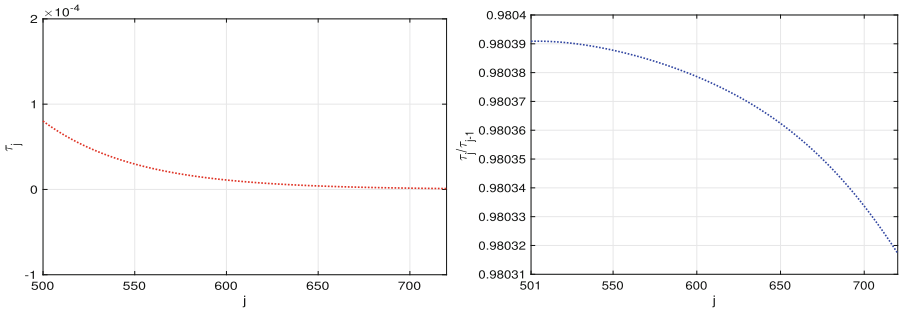

Fig. 4. [LEFT] Adaptive temporal step sizes used in the last 223 excursions of simulations. [RIGHT] Profile of the ratio τ_j/τ_{j-1}, in the final 223 temporal steps. It can be noticed that both τ_j and the ratio decrease monotonically while the $\|q_j\|_\infty$ increases monotonically.

4 Conclusions and Expectations

To conclude, in this paper, we have extended the theory and practice of semi-adaptive finite difference methods for degenerate quenching data stream simulations via nonlinear reaction-diffusion partial differential equations. The particular modeling equation studied is emerged from multiple bio-medical and physical applications, in particular in rapid cell bursts and solid fuel combustion [1,2,4,7,9,13,21,22]. Systematic investigations and improved analysis of key characteristic issues, including the convergence, positivity and monotonicity of the simulated data streams.

Computational experiments are carried out to illustrate the theoretical results though demonstrations of the solution accuracy and order of convergences. It is found that the implicit simulation method implemented is quadratically convergent within the time-space physical regions considered.

The new preservative simulation method utilizes a uniform mesh in space and a temporal adaption in time. In our forthcoming work, we shall implement fully adaptive methods where mesh adaptations will be considered in both space and time. These may help further improve the accuracy and efficiency of the laboratory data. Geometrically non-symmetric degeneracy functions [10,21] and initial values will be introduced and tested for potential biomedical and industrial applications.

References

1. Raghuraman, S., et al.: Pressure drives rapid burst-like coordinated cellular motion from 3D cancer aggregates. Adv. Sci. **9**, 2104808 (2022). https://doi.org/10.1002/advs.202104808
2. Butcher, D., Alliston, T., Weaver, V.: A tense situation: forcing tumour progression. Nat. Rev. Cancer **9**, 108–122 (2009). https://doi.org/10.1038/nrc2544
3. Kawarada, H.: On solutions of initial-boundary value problems for $u_t = u_{xx} + 1/(1-u)$. Publ. Res. Inst. Math. Sci. **10**, 729–736 (1975)

4. Poinset, T., Veynante, D.: Theoretical and Numerical Combustion, 2nd edn. Edwards Publisher, Philadelphia (2005)
5. Sheng, Q., Khaliq, A.: A revisit of the semi-adaptive method for singular degenerate reaction-diffusion equations, East Asia. J. Appl. Math. **2**, 185–203 (2012)
6. Beauregard, M., Sheng, Q.: An adaptive splitting approach for the quenching solution of reaction-diffusion equations over nonuniform grids. J. Comp. Appl. Math. **241**, 30–44 (2013)
7. Bebernes, J., Eberly, D.: Mathematical Problems from Combustion Theory. Springer, New York (1989). https://doi.org/10.1007/978-1-4612-4546-9
8. Bon, T.K., Kouakou, T.K.: Continuity of the quenching time in a semilinear heat equation with a potential. Revista Colombiana de Matemáticas **43**, 55–70 (2009)
9. Zirwes, T., et al.: Numerical study of quenching distances for side-wall quenching using detailed diffusion and chemistry. Flow Turb. Combustion **106**, 649–679 (2021)
10. Acker, A.F., Kawohl, B.: Remarks on quenching. Nonlinear Anal. Theory Meth. Appl. **13**, 53–61 (1989)
11. Hale, J.K.: Asymptotic Behavior of Dissipative Systems. American Math Soc, Philadelphia (1988)
12. Levine, H.A.: Quenching, nonquenching, and beyond quenching for solution of some parabolic equations. Annali di Matematica **155**, 243–260 (1989)
13. Padgett, J.L., Sheng, Q.: Nonuniform Crank-Nicolson scheme for solving the stochastic Kawarada equation via arbitrary grids. Numer. Meth. PDEs **33**, 1305–1328 (2017)
14. Huang, W., Russell, R.D.: Adaptive Moving Mesh Methods. Springer, Zürich (2011)
15. Nouaili, N.: A Liouville theorem for a heat equation and applications for quenching. Nonlinearity **24**, 797–832 (2011)
16. Cheng, H., Lin, P., Sheng, Q., Tan, R.: Solving degenerate reaction-diffusion equations via variable step Peaceman-Rachford splitting. SIAM J. Sci. Comput. **25**(4), 1273–1292 (2003)
17. Sheng, Q., Torres, E.S.: A nonconventional stability approach for a nonlinear Crank-Nicolson method solving degenerate Kawarada problems (2023, submitted and under reviews)
18. Iserles, A.: A First Course in the Numerical Analysis of Differential Equations, 2nd edn. Cambridge University Press, Cambridge and London (2009)
19. Padgett, J.L., Sheng, Q.: On the positivity, monotonicity, and stability of a semi-adaptive LOD method for solving three-dimensional degenerate Kawarada equations. J. Math. Anal. Appls. **439**, 465–480 (2016)
20. Kabre, J., Sheng, Q.: A preservative splitting approximation of the solution of a variable coefficient quenching problem, Computers. Math. Appl. **100**, 62–73 (2021)
21. Sheng, Q., Khaliq, A.: Integral Methods in Science and Engineering (Research Notes in Math), Chapman and Hall/CRC, London and New York (2001). Ch. 9. A monotonically convergent adaptive method for nonlinear combustion problems
22. D. Krndija, et al.: Active cell migration is critical for steady-state epithelial turnover in the gut, Science 365 (2019) 705–710. https://doi.org/10.11268/science.aau3429
23. Zhou, J.: Quenching for a parabolic equation with variable coefficient modeling MEMS technology. App. Math. Comput. **314**, 7–11 (2017)
24. Liang, K., Lin, P., Tan, R.: Numerical solution of quenching problems using mesh-dependent variable temporal steps. App. Numer. Math. **57**, 791–800 (2007)